Fluid Dynamics &
Materials Processing

Tech Science Press

Doi:10.32604/fdmp.2025.064503

ARTICLE

Analytical Investigation of MFD Viscosity and Ohmic Heating in MHD Boundary Layers of Jeffrey Fluid

K. Sinivasan[1], **N. Vishnu Ganesh**[1,*], **G. Hirankumar**[2] **and M. Al-Mdallal Qasem**[3,*]

[1]Post Graduate and Research Department of Mathematics, Ramakrishna Mission Vivekananda College, Mylapore, Chennai, 600004, Tamil Nadu, India
[2]Department of Physics, Ramakrishna Mission Vivekananda College, Mylapore, Chennai, 600004, Tamil Nadu, India
[3]Department of Mathematical Sciences, United Arab Emirates University, Al Ain, P.O. Box 15551, Abu Dhabi, United Arab Emirates

*Corresponding Authors: N. Vishnu Ganesh. Email: ntpvishnuganesh@rkmvc.ac.in;
M. Al-Mdallal Qasem. Email: q.almdallal@uaeu.ac.ae

Received: 17 February 2025; Accepted: 16 April 2025; Published: 30 May 2025

ABSTRACT: In this study, an analytical investigation is carried out to assess the impact of magnetic field-dependent (MFD) viscosity on the momentum and heat transfers inside the boundary layer of a Jeffrey fluid flowing over a horizontally elongating sheet, while taking into account the effects of ohmic dissipation. By applying similarity transformations, the original nonlinear governing equations with partial derivatives are transformed into ordinary differential equations. Analytical expressions for the momentum and energy equations are derived, incorporating the influence of MFD viscosity on the Jeffrey fluid. Then the impact of different parameters is assessed, including magnetic viscosity, magnetic interaction, retardation time, Deborah number, and Eckert number, on the velocity and temperature profiles in the boundary layer. The findings reveal that an increase in magnetic viscosity leads to a decrease in the local Nusselt number, thereby impairing heat transfer. Moreover, a higher retardation time enhances the local Nusselt number by thinning the momentum and thermal boundary layers, while a higher Deborah number decreases the local Nusselt number due to the reduction in fluid viscosity.

KEYWORDS: Analytical solution; heat transfer; Jeffrey fluid; magnetic field-dependent viscosity; magnetohydrodynamics

1 Introduction

In recent years, interest in the flow behavior of non-Newtonian fluids has increased, particularly in boundary layer flows caused by a stretching surface with heat transfer. This interest stems from their wide-ranging engineering and industrial applications, such as the cooling of metallic plates, glass blowing, continuous casting and filament extrusion, polymer or rubber sheet, and the aerodynamic extrusion of plastic sheets, where the rate of cooling has a significant impact on the quality of the final product [1–3]. It is widely recognized that Newton's viscosity law is insufficient for characterizing the flow behavior of complex fluids, which cannot be studied using a single governing equation that relates stress to the rate of deformation [4,5]. This limitation has prompted the investigation of various constitutive models in the literature [6–9].

The Jeffrey fluid, a non-Newtonian model, enhances the Newtonian framework by incorporating time derivatives to account for relaxation and retardation times. This model is commonly applied to complex fluids, such as polymer melts, blood, suspension systems, lubricants, mud, slurries, and certain biological fluids like synovial fluid, where the flow exhibits viscoelastic behavior [10–12]. The integration of magnetohydrodynamics (MHD), Jeffrey fluid dynamics, and ohmic dissipation enhances heat transfer, flow behavior, and energy efficiency in electrically conducting non-Newtonian fluids across applications in metallurgy, lubrication, biomedical systems, space science, energy generation, and environmental engineering [13–15]. Various numerical studies have explored the intersection of MHD and Jeffrey fluid heat transfer, analyzing the effects of different physical factors, including Joule heating [16], viscous dissipation [17], heat sources and sinks [18], entropy generation [19], thermal radiation [20], chemical reactions [21], activation energy [22], porous media [23], nanoparticles [24], and inclined plates [25], among others [26–29]. Apart from these numerical studies, considerable interest has been directed towards the analytical investigation of the MHD Jeffrey fluid boundary layer problem, which provides valuable mathematical insight into the governing equations and their solutions. For instance, Alsaedi et al. [30] analytically examined the two-dimensional MHD flow of Jeffrey fluid with convective boundary conditions and chemical reactions on a stretching sheet, employing the Gamma function to obtain solutions. Ahmed et al. [31] analytically investigated convective heat transfer in magnetohydrodynamic (MHD) Jeffrey fluid flow over an extending surface, accounting for Joule and viscous dissipation, internal heat generation/absorption, and radiative heat transfer using confluent hypergeometric functions. Hayat et al. [32] performed an analytical study on MHD stagnation-point flow of Jeffrey fluid over a heated stretched sheet using the homotopy analysis method, noting dual behavior in the velocity ratio. Turkyilmazoglu [33] analytically investigated MHD slip flow and heat transfer at a stagnation point flow of Jeffrey fluid over deformable surfaces, focusing on the existence and uniqueness of solutions while emphasizing magnetic interaction. Kumar et al. [34] analytically investigated the influence of Joule heating on mixed convection MHD flow of an incompressible Jeffrey fluid, incorporating power-law heat flux and suction, through the homotopy analysis method. Nisar et al. [35] analytically analyzed steady free convective flow of electrically conducting Jeffrey fluid over a stretching surface, utilizing the Adomian Decomposition Method for approximate solutions.

Magnetic-field-dependent (MFD) viscosity describes the impact of magnetic fields on fluid flow by altering viscosity through interactions with charged particles. Accurate models incorporating MFD viscosity are essential for optimizing conducting fluid flows in plasma physics, engineering, astronomy, and industry [36]. The effects of MFD viscosity on heat transfer and fluid flow were studied in various contexts [37,38]. The effect of MFD viscosity on the Casson fluid boundary layer over a stretching sheet was numerically investigated [39], and an analytical study on second-grade fluid boundary layer flow over a stretching sheet was conducted by Ganesh et al. [40]. However, investigations into the effect of MFD viscosity on Jeffrey fluid flow in any physical setting were not reported either numerically or analytically in the literature.

To address this gap, the present analytical study focuses on examining the heat transfer behavior of Jeffrey fluids on a horizontally stretched sheet with MFD viscosity and ohmic dissipation, with potential applications in plasma physics, material processing, energy systems, and biomedical engineering, where controlling fluid behavior under magnetic fields is essential for optimizing heat transfer, enhancing flow stability, and improving system efficiency. The mathematical model incorporates both energy and momentum equations, accounting for the effects of MFD viscosity. These equations are solved analytically, providing new insights into the interaction between MFD viscosity and the flow. The heat equation is analyzed under two boundary conditions: prescribed heat flux (PHF) and prescribed surface temperature (PST). The study examines the influence of fundamental parameters, including the Deborah number, Eckert number, retardation time, magnetic viscosity, and magnetic interaction, on crucial physical characteristics such as velocity, skin friction, temperature distribution, and the local Nusselt number.

The primary objective of this study is to explore the following:

- Determining whether an analytical solution for Jeffrey fluid is possible with magnetic field-dependent viscosity and Joule heating.
- Examining the impact of magnetic field-dependent viscosity on the velocity and temperature profiles of Jeffrey fluid.
- Analyzing the behavior of PST and PHF cases in the temperature profile under the influence of magnetic field-dependent viscosity.
- Investigating the behavior of skin friction and the local Nusselt number in the presence of magnetic field-dependent viscosity.

2 Problem Structure

Assume the steady, laminar, two-dimensional boundary layer motion of an incompressible MHD Jeffrey fluid flowing past a stretching surface parallel to the reference plane $y = 0$. The magnetic field strength B_0 is applied normally to the sheet. For small magnetic Reynolds numbers, the induced magnetic field is supposed to be minimal compared to the applied magnetic field. The stretched sheet has a velocity of $u^* = dbx$ (where b is a constant and $d = 1$ for stretching sheet). The flow is restricted to $y > 0$. In the Cartesian coordinate system, the x and y axes are aligned parallel and perpendicular to the sheet, in this order (see Fig. 1). The constitutive relation for a Jeffrey fluid is stated as (see [2,4]).

$$\tau^* = A - Ip, \tag{1}$$

$$A = \frac{\eta^*}{\lambda_1 + 1}\left(\lambda_2\left(\nabla \cdot \overline{V} + \frac{\partial R_1}{\partial t}\right) R_1 + R_1\right), \tag{2}$$

$$\mathrm{R}_1 = \left(\nabla \overline{V}\right)^{t^*} + \left(\nabla \overline{V}\right). \tag{3}$$

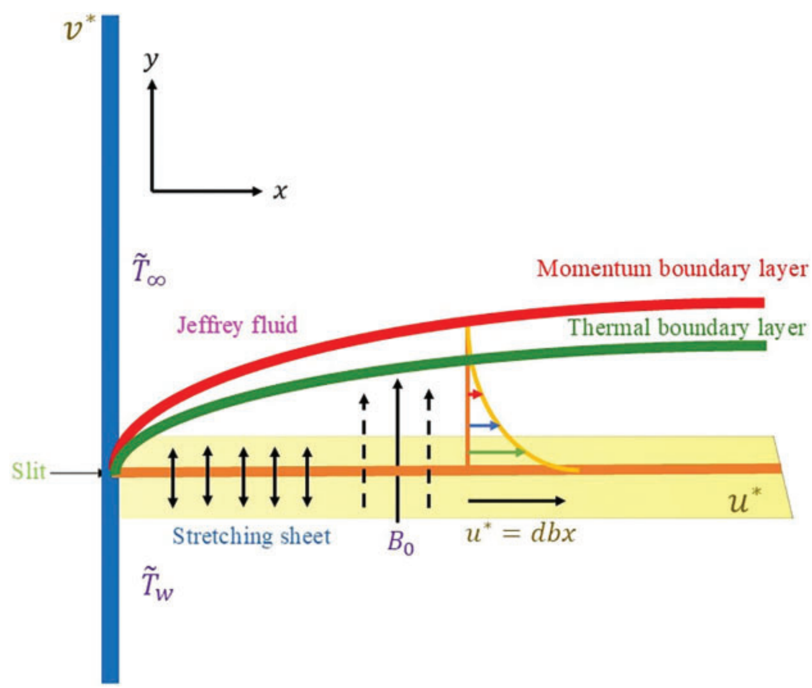

Figure 1: Physical configuration of Jeffrey fluid over a stretching sheet

The problem formulation explicitly considers the influences of MFD viscosity and Ohmic dissipation while neglecting viscous dissipation and thermal radiation effects. The equations governing the present problem for velocity and temperature field subject to boundary layer approximation are given by the following equations (see [10,31]):

$$\frac{\partial v^*}{\partial y}+\frac{\partial u^*}{\partial x}=0, \tag{4}$$

$$v^*\frac{\partial u^*}{\partial y}+u^*\frac{\partial u^*}{\partial x}=\frac{\eta^*}{\rho}\frac{1}{\lambda_1+1}\left(\frac{\partial^2 u^*}{\partial y^2}+\lambda_2\left(v^*\frac{\partial^3 u^*}{\partial y^3}+u^*\frac{\partial^3 u^*}{\partial x\partial y^2}-\frac{\partial u^*}{\partial x}\frac{\partial^2 u^*}{\partial y^2}+\frac{\partial u^*}{\partial y}\frac{\partial^2 u^*}{\partial x\partial y}\right)\right)-\frac{\sigma B_0^2}{\rho}u^*, \tag{5}$$

$$u^*\frac{\partial \tilde{T}}{\partial x}+v^*\frac{\partial \tilde{T}}{\partial y}=\frac{\kappa}{\rho c_p}\frac{\partial^2 \tilde{T}}{\partial y^2}+\frac{\sigma B_0^2 u^{*2}}{\rho c_p}. \tag{6}$$

This fluid flow consists of the corresponding boundary conditions (see [31])

$$u^*=xbd,\quad v^*=v_w,\quad \text{at}\quad y=0,\ \lim_{y\to\infty}u^*=0, \tag{7}$$

$$\tilde{T}=\tilde{T}_w=\tilde{T}_\infty+A_0\left(\frac{x}{l}\right)^2\quad \text{at}\quad y=0,\ \lim_{y\to\infty}\tilde{T}=\tilde{T}_\infty\ (\text{PST Case}), \tag{8}$$

$$-\kappa\left(\frac{\partial \tilde{T}}{\partial y}\right)_w=q_w=E_0\left(\frac{x}{l}\right)^2\quad \text{at}\quad y=0,\ \lim_{y\to\infty}\tilde{T}=\tilde{T}_\infty\ (\text{PHF Case}). \tag{9}$$

The viscosity of the Jeffrey fluid is characterized by a linear variation with the magnetic field, as referenced in [38–40].

$$\eta^*=\left(\overline{B}_0\bullet\overline{\delta}+1\right)\mu, \tag{10}$$

where $\overline{B}_0=B_{0x}\overline{e}_x+B_{0y}\overline{e}_y$ with $B_{0x}=B_{0y}=B_0$ and $\overline{\delta}=\delta_x\overline{e}_x+\delta_y\overline{e}_y$ with $\delta=\delta_y=\delta_x$, indicating the isotropic variation in viscosity due to the magnetic field.

The Eq. (10) can be simplified to

$$\eta^*=(1+\delta^*)\mu,$$

where $\delta^*=\delta B_0$.

The similarity variable is defined as (see [2,3,40])

$$\begin{gathered}\eta=\sqrt{\frac{b}{v}}y,\quad \psi(x,y)=\sqrt{bv}\,xF(\eta),\\ \Theta=\frac{\tilde{T}-\tilde{T}_\infty}{\tilde{T}_w-\tilde{T}_\infty}\ (\text{PST case}),\quad G=\frac{\tilde{T}-\tilde{T}_\infty}{\tilde{T}_w-\tilde{T}_\infty}\ (\text{PHF case}),\end{gathered} \tag{11}$$

$$u^*=\frac{\partial\psi}{\partial y}=bxF_\eta(\eta),\quad v^*=-\frac{\partial\psi}{\partial x}=-\sqrt{bv}\,F(\eta). \tag{12}$$

The velocity components are defined in Eq. (12) and naturally satisfy the requirements given in Eq. (4).

3 Analytical Solution of Momentum Equations

Using the non-dimensional similarity variable Eqs. (11) and (12) in the PDE Eq. (5), the following ODE equation is obtained (see [9])

$$(\lambda_1+1)\left(-QF_\eta-\left(F_\eta\right)^2+FF_{\eta\eta}\right)+(\delta^*+1)\left(F_{\eta\eta\eta}+\left(-FF_{\eta\eta\eta\eta}+\left(F_{\eta\eta}\right)^2\right)\beta\right)=0, \tag{13}$$

with the boundary conditions

$$\begin{aligned}&F(0)=-\frac{v_w}{\sqrt{bv}}=S,\quad F_\eta(0)=d,\quad \text{at}\ \eta=0,\\&\lim_{\eta\to\infty}F_\eta(\eta)=0,\end{aligned} \tag{14}$$

where $\beta=\lambda_2 b$ is the Deborah number behaves in three different ways: when $\beta<1$, it behaves like a fluid; when $\beta=1$, it behaves like a viscoelastic fluid; and when $\beta>1$, it behaves like a solid.

Applying the boundary conditions (14), the exact solution to Eq. (13) is found as follows:

$$F(\eta)=S+\left(\frac{d-de^{-\alpha\eta}}{\alpha}\right), \tag{15}$$

by substituting Eqs. (15) into (13), the following cubic algebraic equation is obtained

$$\alpha^3+\frac{(1+\beta d)}{\beta S}\alpha^2-\frac{(1+\lambda_1)}{(1+\delta^*)\beta}\alpha-\frac{(Q+d)(1+\lambda_1)}{(1+\delta^*)\beta S}=0, \tag{16}$$

upon solving Eq. (16), three expressions for α are derived

$$\alpha_1=l+\frac{p}{3\times 2^{\frac{1}{3}}}-\frac{2^{\frac{1}{3}}m}{3p}, \tag{17}$$

$$\alpha_2=l+\frac{\left(i\sqrt{3}+1\right)m}{3p\times 2^{\frac{2}{3}}}-\frac{\left(-i\sqrt{3}+1\right)p}{2^{\frac{1}{3}}\times 6}, \tag{18}$$

$$\alpha_3=l+\frac{\left(-i\sqrt{3}+1\right)m}{3p\times 2^{\frac{2}{3}}}-\frac{\left(i\sqrt{3}+1\right)p}{2^{\frac{1}{3}}\times 6}, \tag{19}$$

where

$$\begin{aligned}&l=-\frac{(1+\beta d)}{3\beta S},\quad \mathrm{m}=-9l^2-\frac{3(1+\lambda_1)}{(1+\delta^*)\beta},\\&\mathrm{n}=54l^3+27\frac{l(1+\lambda_1)}{(1+\delta^*)\beta}+27\frac{(1+\lambda_1)(Q+d)}{(1+\delta^*)\beta S},\quad p=\left(n+\sqrt{4m^3+n^2}\right)^{\frac{1}{3}}.\end{aligned} \tag{20}$$

The skin friction coefficient, C_f is defined (see [5,6]) as

$$C_f=\frac{\tau_w}{\frac{1}{2}\rho u_w^2},\text{where}\ \tau_w=\frac{\eta^*}{1+\lambda_1}\left(\frac{\partial u^*}{\partial y}+\lambda_2\left(u^*\frac{\partial^2u^*}{\partial x\partial y}+v^*\frac{\partial^2u^*}{\partial y^2}\right)\right)_{y=0}. \tag{21}$$

Using the similarity variables Eqs. (11) and (12) in Eq. (21). The skin friction is obtained as

$$\frac{(\lambda_1+1)\,C_f d^2 \mathrm{Re}_x^{\frac{1}{2}}}{2} = (\delta^*+1)\left(\beta\left(-F(0)\,F_{\eta\eta\eta}(0)+F_{\eta\eta}(0)\,F_\eta(0)\right)+F_{\eta\eta}(0)\right). \tag{22}$$

where $\mathrm{Re}_x = \dfrac{bx^2}{\nu}$ represents the local Reynolds number.

4 Analytical Solution of Energy Equations

4.1 Heat Transfer in the Prescribed Surface Temperature (PST) Case

The energy PDE in Eq. (6) and PST boundary conditions are converted into a non-dimensional ODE and non-dimensional boundary condition using Eqs. (11) and (12) as follows:

$$\Theta_{\eta\eta} + \Pr F\Theta_\eta - 2\Pr F_\eta\Theta = -\Pr Ec_1 Q F_\eta^2, \tag{23}$$

$$\Theta(0) = 1 \quad \text{and} \quad \Theta(\infty) = 0. \tag{24}$$

Upon introducing the new variable $\xi = -\dfrac{e^{-\eta\alpha}\Pr}{\alpha^2}$ into Eqs. (23) and (24), we get

$$2d\Theta + \left(-\xi d - a^{\#}{}_0 + 1\right)\Theta_\xi + \xi\Theta_{\xi\xi} = -\frac{Ec_1\alpha^2 d^2 Q\xi}{\Pr}, \tag{25}$$

$$\Theta\left(-\frac{\Pr}{\alpha^2}\right) = 1 \quad \text{and} \quad \Theta(0) = 0. \tag{26}$$

where $a^{\#}{}_0 = \dfrac{\Pr d}{\alpha^2} + \dfrac{\Pr S}{\alpha}$.

The analytical solution of Eq. (25), subject to the boundary condition (26), is expressed in terms of the confluent hypergeometric function as a function of ξ as

$$\Theta(\xi) = \left(\frac{1+\dfrac{Ec_1\Pr d^2}{\alpha^2}\dfrac{Q}{2\left(2-a^{\#}{}_0\right)}}{M\left(a^{\#}{}_0-2, 1+a^{\#}{}_0, \dfrac{-\Pr}{\alpha^2}d\right)\left(\dfrac{-\Pr}{\alpha^2}\right)^{a^{\#}{}_0}}\right)\xi^{a^{\#}{}_0} M\left(a^{\#}{}_0-2, 1+a^{\#}{}_0, \xi d\right) + \left(-\frac{Ec_1\alpha^2 d^2}{\Pr}\frac{Q}{2\left(2-a^{\#}{}_0\right)}\xi^2\right). \tag{27}$$

Upon replacing the variable ξ with η, we get

$$\Theta(\eta) = (-C_1+1)\,e^{-a^{\#}{}_0\alpha\eta} \times \frac{M\left(a^{\#}{}_0-2, 1+a^{\#}{}_0, \dfrac{-\Pr d}{\alpha^2}e^{-\alpha\eta}\right)}{M\left(a^{\#}{}_0-2, 1+a^{\#}{}_0, \dfrac{-\Pr d}{\alpha^2}\right)} + C_1 e^{-2\alpha\eta}. \tag{28}$$

The dimensionless gradient of the wall temperature for the PST case is given by $\Theta_\eta(0)$ is

$$\Theta_\eta(0) = (1-C_1)\left(\frac{\Pr d}{\alpha}\frac{a^{\#}{}_0-2}{1+a^{\#}{}_0} \times \frac{M\left(a^{\#}{}_0-1, 2+a^{\#}{}_0, \dfrac{-\Pr d}{\alpha^2}\right)}{M\left(a^{\#}{}_0-2, 1+a^{\#}{}_0, \dfrac{-\Pr d}{\alpha^2}\right)} - a^{\#}{}_0\alpha\right) - 2C_1\alpha. \tag{29}$$

where $C_1 = -\dfrac{Ec_1 \Pr d^2 Q}{2\alpha^2 \left(2 - a^{\#}{}_0\right)}$, and M is the Confluent Hypergeometric function [40] defined by

$$M\left(\tilde{a}, \tilde{b}, x\right) = 1 + \sum_{n=1}^{\infty} \frac{\left(\tilde{a}\right)_n x^n}{\left(\tilde{b}\right)_n n!},$$
$$\left(\tilde{a}\right)_n = \tilde{a}_0 \left(1 + \tilde{a}_0\right)\left(2 + \tilde{a}_0\right), \cdots, \left(n - 1 + \tilde{a}_0\right),$$
$$\left(\tilde{b}\right)_n = \tilde{b}_0 \left(1 + \tilde{b}_0\right)\left(2 + \tilde{b}_0\right), \cdots, \left(n - 1 + \tilde{b}_0\right).$$

The local Nusselt number, as defined in [31,40], is Nu_1 for PST case

$$Nu_1 = \frac{x q_w}{\kappa\left(\tilde{T}_w - \tilde{T}_\infty\right)}, \quad \text{Where} \quad q_w = -\kappa\left(\frac{\partial \tilde{T}}{\partial y}\right)_{y=0}. \tag{30}$$

Using the similarity variables in Eqs. (11), (30) yields the following equation:

$$Nu_1 \operatorname{Re}_x^{-\left(\frac{1}{2}\right)} = -\Theta_\eta (0). \tag{31}$$

4.2 Heat Transfer in the Prescribed Surface Heat Flux (PHF) Case

The energy PDE in Eq. (6) and PHF boundary conditions are converted into a non-dimensional ODE and non-dimensional boundary condition using Eqs. (11) and (12) as follows:

$$G_{\eta\eta} + \Pr F G_\eta - 2 \Pr F_\eta G = -\Pr Ec_2 Q F_\eta^2, \tag{32}$$
$$G_\eta (0) = -1 \quad \text{and} \quad G(\infty) = 0. \tag{33}$$

Substituting ξ into Eqs. (32) and (33) yields

$$2dG + \left(-\xi d - a^{\#}{}_0 + 1\right) G_\xi + \xi G_{\xi\xi} = -\frac{Ec_2 \alpha^2 d^2 Q \xi}{\Pr}, \tag{34}$$

$$G_\xi\left(-\frac{\Pr}{\alpha^2}\right) = -\frac{\alpha}{\Pr} \quad \text{and} \quad G(0) = 0. \tag{35}$$

The analytical solutions of Eqs. (34) with (35) are expressed in terms of ξ and η as

$$G(\xi) = \left(\frac{-\dfrac{\alpha}{\Pr} - \dfrac{Ec_2 d^2 Q}{\left(2 - a^{\#}{}_0\right)}}{\left(\left(\left(\dfrac{a^{\#}{}_0 - 2}{1 + a^{\#}{}_0}\right) d M\left(a^{\#}{}_0 - 1, 2 + a^{\#}{}_0, \dfrac{-\Pr}{\alpha^2} d\right) + a^{\#}{}_0 M\left(a^{\#}{}_0 - 2, 1 + a^{\#}{}_0, \dfrac{-\Pr}{\alpha^2} d\right)\left(\dfrac{-\alpha^2}{\Pr}\right)\right)\left(\dfrac{-\alpha^2}{\Pr}\right)^{-a^{\#}{}_0}}\right)$$
$$\times\, \xi^{a^{\#}{}_0} M\left(a^{\#}{}_0 - 2, 1 + a^{\#}{}_0, d\xi\right) - \frac{Ec_2 \alpha^2 d^2}{\Pr} \frac{Q}{2\left(2 - a^{\#}{}_0\right)} \xi^2, \tag{36}$$

$$G(\eta) = C_2 e^{-a^{\#}{}_0 \alpha \eta}\ M\left(a^{\#}{}_0 - 2, 1 + a^{\#}{}_0, \frac{-\Pr d}{\alpha^2} e^{-\alpha\eta}\right) + C_1 e^{-\eta 2\alpha}. \tag{37}$$

The dimensionless gradient of the wall temperature for the PHF case is given by

$$G\ (0) = C_2 M\left(a^{\#}{}_0 - 2, 1 + a^{\#}{}_0, \frac{-\Pr d}{\alpha^2}\right) + C_1. \tag{38}$$

where

$$C_2 = \frac{(-1 + 2C_1\alpha)}{\left(-\alpha a^{\#}{}_0 M\left(a^{\#}{}_0 - 2, 1 + a^{\#}{}_0, \frac{-\Pr}{\alpha^2} d\right) + \left(\frac{a^{\#}{}_0 - 2}{1 + a^{\#}{}_0}\right) d \frac{\Pr}{\alpha} M\left(a^{\#}{}_0 - 1, 2 + a^{\#}{}_0, \frac{-\Pr d}{\alpha^2}\right)\right)}$$

The local Nusselt number is defined (see [31,40]) as Nu_2 for PHF case

$$Nu_2 = \frac{x\left(\frac{\nu}{b}\right) q_w}{\kappa\left(\tilde{T}_w - \tilde{T}_\infty\right)}, \quad \text{Where} \quad q_w = E_0\left(\frac{1}{l^2}\right)_{y=0}. \tag{39}$$

Using the similarity variable and the PHF boundary condition in Eq. (39) yields the following equation:

$$Nu_2 \operatorname{Re}_x^{-\left(\frac{1}{2}\right)} = \frac{1}{G(0)}. \tag{40}$$

5 Results and Discussion

To verify the analytical expressions, the outcomes of $F_{\eta\eta}(0)$ are compared with those presented by Dalir [8] and listed in Table 1 for different values of β and λ_1, without considering MFD viscosity and ohmic dissipation. Table 1 presents the relevant data, indicating a high level of agreement between the outcomes. The impacts of several key parameters on velocity and temperature profiles, namely the magnetic viscosity parameter (δ^*), magnetic interaction parameter (Q), retardation time (λ_1), Deborah number $(\beta = \lambda_2 b)$, Eckert number $(Ec = Ec_1 = Ec_2)$, and Prandtl number $(\Pr)$, are presented through graphical representations of the velocity and temperature profiles. Throughout the study, the parameters were maintained at fixed values: $d = 1$, $\lambda_1 = 0.5$, $\delta^* = 0.5$, $\beta = 0.5$, $Q = 1$, $S = 2$, $Ec = 2$, and $\Pr = 3$ based on the previous literature [8,34]. The subsequent sections will elaborate on the obtained results.

Table 1: Comparison values of $F_{\eta\eta}(0)$ for several values of β and λ_1 when $\delta = Q = Ec = 0$, $S = 0.00001$, $d = 1$ and $\Pr = 0.71$

$F_{\eta\eta}(0)$ for Various β: $\lambda_1 = 0.2$			$F_{\eta\eta}(0)$ for Various λ_1: $\beta = 0.2$		
β	Dalir [8]	Present result	λ_1	Dalir [8]	Present result
0.4	−0.92582010	−0.9258233	0.4	−1.08012345	−1.0801287
0.6	−0.86602540	−0.8660276	0.6	−1.15470054	−1.1547068
1.0	−0.77459667	−0.7745983	1.0	−1.29099445	−1.2910027
1.4	−0.70710678	−0.7071082	1.4	−1.41421356	−1.4142228
1.6	−0.67936622	−0.6793673	1.6	−1.47196014	−1.4719694
2.0	−0.63245553	−0.6324561	2.0	−1.58113883	−1.5811500
2.4	−0.59408853	−0.5940891	2.4	−1.68325082	−1.6832631
2.6	−0.57735027	−0.5773509	2.6	−1.73205081	−1.7320640
3.0	−0.54772256	−0.5477230	3.0	−1.82574186	−1.8257569

5.1 Results for the Momentum Equation Solution

The boundary constraints stated in Eq. (14) are used to determine the precise solution to the dimensionless momentum equation. This solution contains an unknown parameter, denoted as α, which needs to be identified to resolve Eq. (13). By substituting Eq. (15) into expression (13), the momentum expression transforms into a cubic polynomial equation (see Eq. (16)) with respect to α. According to the fundamental theorem of algebra, solving for α yields three solutions for Eq. (13), denoted as α_1, α_2 and α_3. It is vital to emphasize that only positive values of α offer physically relevant solutions to this problem [5,33,40].

Fig. 2 depicts the physically viable solution α corresponding to the momentum equation in relation to the suction parameter (S). It is observed that only one of the values α_1, α_2 and α_3, considered α_1 provides a meaningful solution. Therefore, there is only one solution to the momentum equation for the current problem. The solution α_1 was employed to obtain exact answers to both the momentum and heat energy equations. Furthermore, Fig. 2a shows that the α_1 value increases as the λ_1 increases. From Fig. 2b,c, it is also noted that the α_1 value drops as the β and δ^* increase. The impact of the Q is shown in Fig. 2d; as the Q increases, so does the α_1 value.

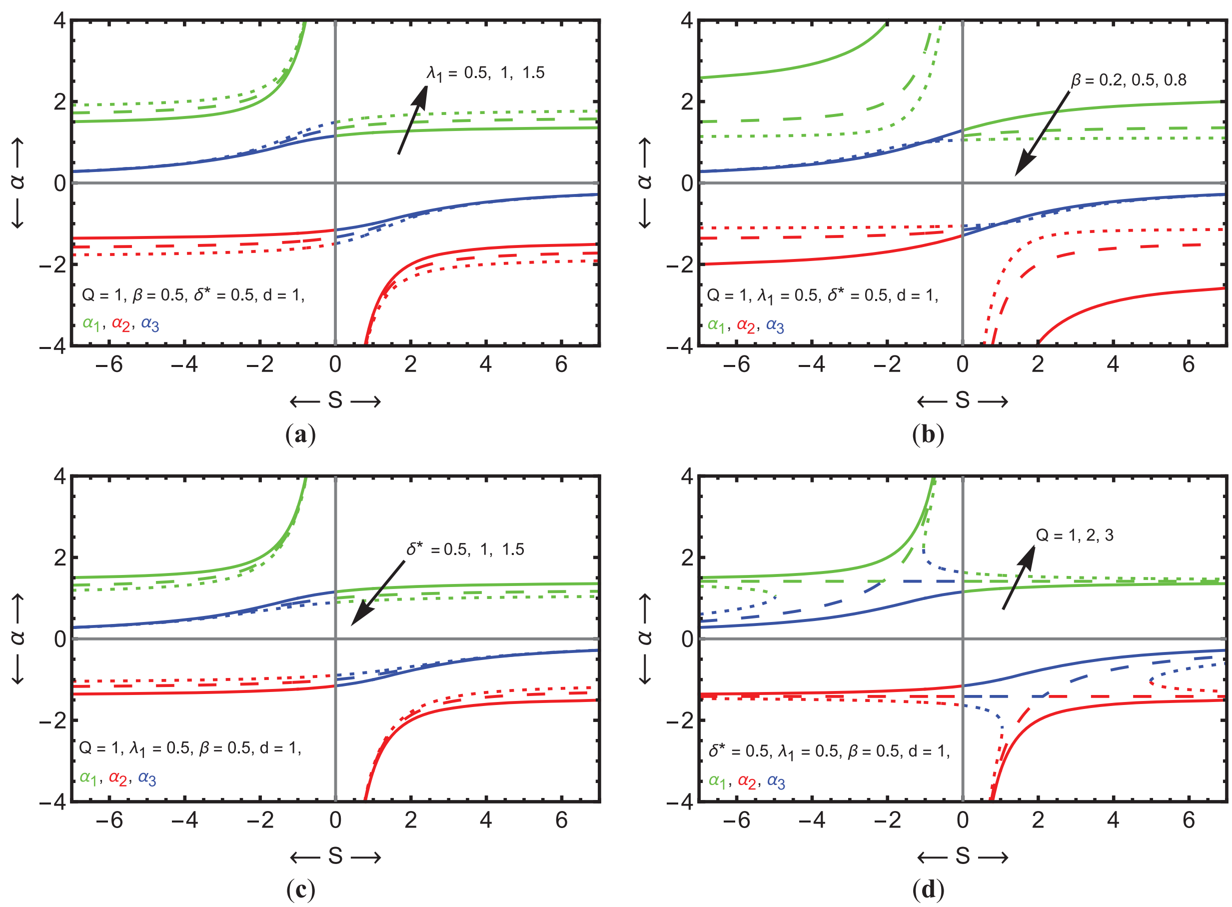

Figure 2: (**a**) Impact of λ_1 on α as a function of S; (**b**) Impact of β on α as a function of S; (**c**) Impact of the δ^* on α as a function of S; (**d**) Impact of Q on α as a function of S

5.2 Analysis of the Velocity Profile

The velocity profile of the Jeffrey fluid for various values, considering the combined effects of λ_1, β, and Q with δ^*, is graphically illustrated in Fig. 3a–c, respectively. Fig. 3a presents a comparative analysis of the λ_1 and the δ^*. It is observed that the fluid's velocity decreases with an increase in λ_1, which is attributed to the thinning of the momentum boundary layer. Conversely, the fluid's velocity rises with an increase in the δ^*, highlighting the magnetic field's influence on the fluid's viscosity. The physical reason for the thinning effect due to increased λ_1 can be linked to the structural changes in the fluid's molecular level interaction. As the λ_1 increases, the fluid molecules experience a delayed viscous response to applied stress, allowing them more time to align and stretch along the flow direction, which reduces the overall resistance, thins the momentum boundary layer, and decreases the velocity.

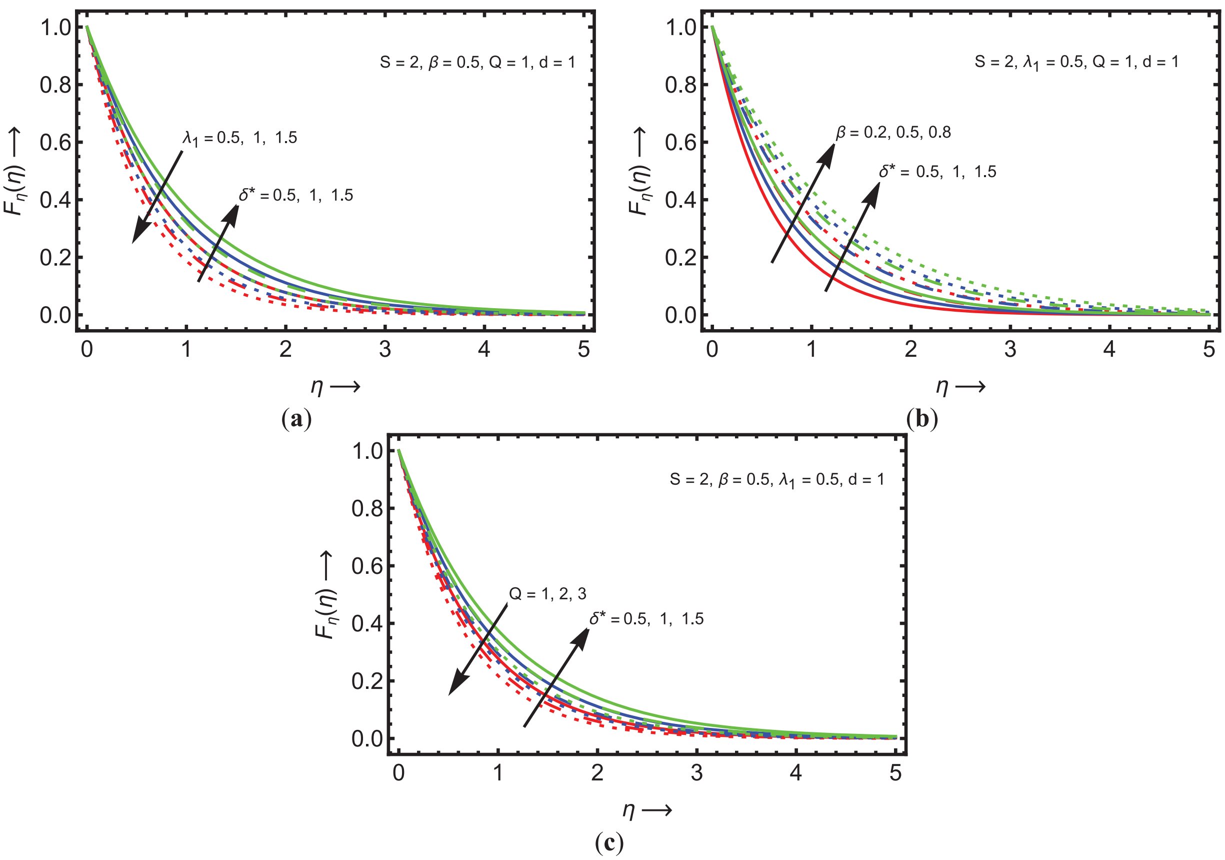

Figure 3: (**a**) Impact of δ^* and λ_1 on $F_\eta(\eta)$. Where colours show δ^* variation and different types of lines show λ_1 variation; (**b**) Impact of δ^* and β on $F_\eta(\eta)$. Where colours show δ^* variation and different types of lines show β variation; (**c**) Impact of δ^* and Q on $F_\eta(\eta)$. Where colours show δ^* variation and different types of lines show Q variation

Fig. 3b displays the effects of the β and the δ^* on the velocity profile. An increase in the β enhances both the fluid velocity and the momentum boundary layer thickness. Since the β is related to the stretching parameter b, it indicates that a higher β corresponds to a greater rate of stretching of the sheet, which in turn reduces the fluid's resistance to motion. This results in higher fluid mobility within the boundary layer near the surface, leading to increased velocity and boundary layer thickness. Furthermore, the increase in magnetic viscosity parameter also boosts the fluid's velocity, compounding with the effects of the β.

The combined impact of the Q and the δ^* on the velocity profile is shown in Fig. 3c. An increase in the Q results in a reduction of the velocity distribution. This decrease in the velocity profile is due to the Lorentz magnetohydrodynamic drag force, which acts perpendicular to the magnetic field and inhibits the flow, whereas an increase in the δ^* enhances the fluid velocity.

5.3 Results on the Skin Friction Coefficient

The local skin friction coefficient is illustrated in Fig. 4 for various values of λ_1, β, and δ^*. The x-axis represents the Q, and the y-axis represents the local skin friction coefficient. The skin friction coefficient decreases as Q rise, while it increases with the increase of λ_1 (Fig. 4a). This occurs because the fluid takes longer to reach its equilibrium state; thus, the increased movement within the fluid generates more friction, leading to a higher skin friction coefficient. Fig. 4b illustrates the influence of the β on the local skin friction coefficient. It is observed that a rise in the β results in a diminish in the local skin friction coefficient. This is because the β is directly proportional to the rate of stretching of the sheet, and a higher β decreases the resistance to fluid motion, thereby reducing the local skin friction coefficient. The impact of the δ^* on the local skin friction coefficient is shown in Fig. 4c. An increase in the δ^* leads to a decrease in the local skin friction coefficient. The relationship between local skin friction coefficient and various parameters, including λ_1, β, δ^*, and Q, is tabulated in Table 2. The computed numerical values of these physical quantities are systematically presented in a tabular format, providing a quantitative perspective that will be useful for future reference.

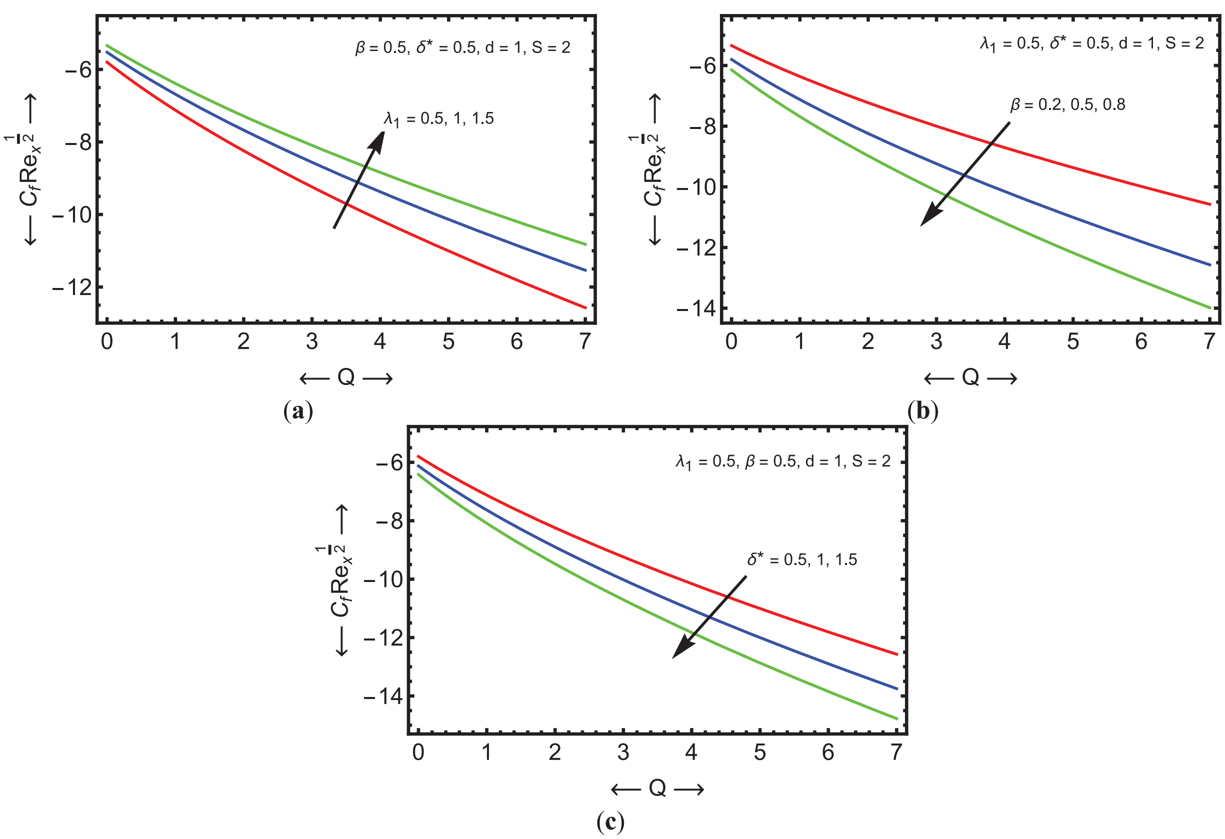

Figure 4: (**a**) Impact of λ_1 on the skin friction $C_f\mathrm{Re}_x^{1/2}$ as Q on the x-axis; (**b**) Impact of β on the skin friction $C_f\mathrm{Re}_x^{1/2}$ as Q on the x-axis; (**c**) Impact of δ^* on the skin friction $C_f\mathrm{Re}_x^{1/2}$ as Q on the x-axis

Table 2: Numerical values of $-F_{\eta\eta}(0)$ and $-C_f \mathrm{Re}_x^{1/2}$ for various values of λ_1, β, δ^* and Q

Parameters	Values	$-F_{\eta\eta}(0)$	$-C_f \mathrm{Re}_x^{1/2}$
λ_1	0.5	1.2807764	7.1231056
	1.0	1.4902246	6.6841592
	1.5	1.6758708	6.3868189
β	0.2	1.6939948	6.3612823
	0.5	1.2807764	7.1231056
	0.8	1.0859694	7.6833449
δ^*	0.5	1.2807764	7.1231056
	1.0	1.1007362	7.6339316
	1.5	0.9787451	8.0868658
Q	1.0	1.2807764	7.1231056
	2.0	1.4142136	8.2426407
	3.0	1.5265672	9.2405162

5.4 Analysis of the Temperature Profile

The temperature profile is analyzed under two separate boundary conditions: the PST and PHF cases. In this context, PST and PHF are represented by different symbols $\Theta(\eta)$ and $G(\eta)$. The temperature profile incorporates the effects of ohmic dissipation, introducing the δ^* and Q into the non-dimensional energy equation. Fig. 5 illustrates the combined effects of λ_1 and the δ^* on the temperature profile for the PST case in Fig. 5a and the PHF case in Fig. 5b. As the λ_1 increases, the temperature profile decreases, which occurs because higher λ_1 thins the thermal boundary layer, reducing the temperature. However, an increase in the δ^* raises the temperature due to the influence of the magnetic field in the fluid, affecting both the PST and PHF cases.

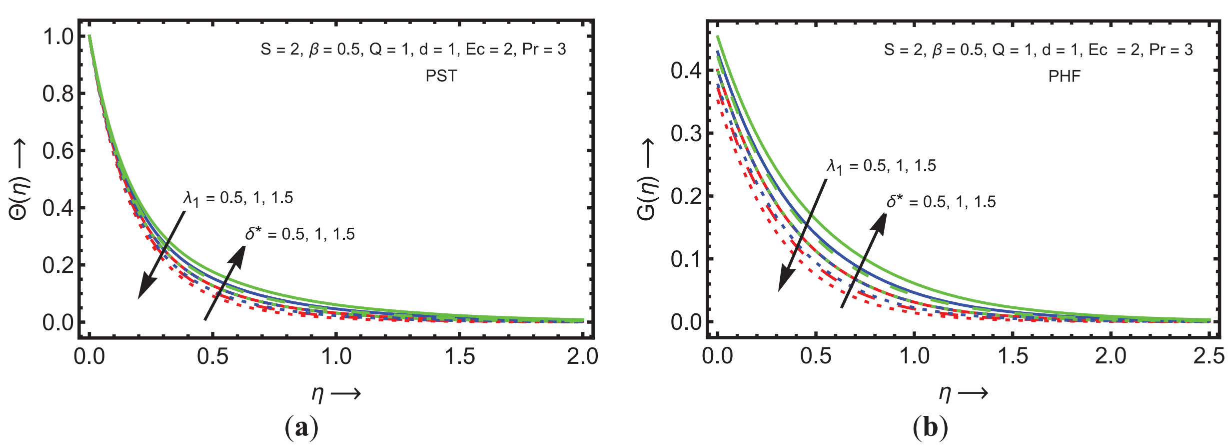

Figure 5: (**a**) Impact of δ^* and λ_1 on $\Theta(\eta)$. Where colours show δ^* variation and different types of lines show λ_1 variation; (**b**) Impact of δ^* and λ_1 on $G(\eta)$. Where colours show δ^* variation and different types of lines show λ_1 variation

Fig. 6 illustrates the combined effects of the β and the δ^* on the temperature profile for both boundary conditions. A rise in the β and δ^* leads to higher temperature profiles (Fig. 6a,b). This effect is due to the intensified motion of fluid particles, which thickens the thermal boundary layer. The enhanced fluid motion slightly raises the temperature at the sheet surface, particularly as the β increases. Additionally, the rise in the δ^* promotes smoother fluid flow, further increasing the thermal boundary layer thickness and temperature.

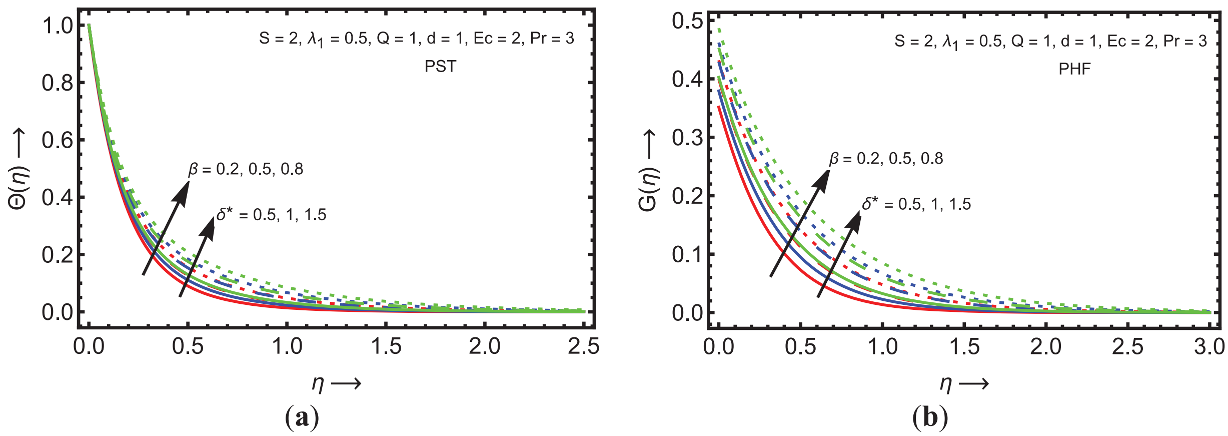

Figure 6: (**a**) Impact of δ^* and β on $\Theta(\eta)$. Where colours show δ^* variation and different types of lines show β variation; (**b**) Impact of δ^* and β on $G(\eta)$. Where colours show δ^* variation and different types of lines show β variation

Fig. 7 shows the temperature profile for the PST and PHF cases, considering the effects of the Q and δ^*. In both Fig. 7a,b, the profiles show an increase in temperature for the PST and PHF cases, due to the effect of the magnetic field. An increase in Q causes the expansion of the flow region in both scenarios. This expansion results from the resistive Lorentz force induced when a transverse magnetic field interacts with an electrically conducting fluid, reducing fluid velocity in the flow region and enhancing the temperature distribution.

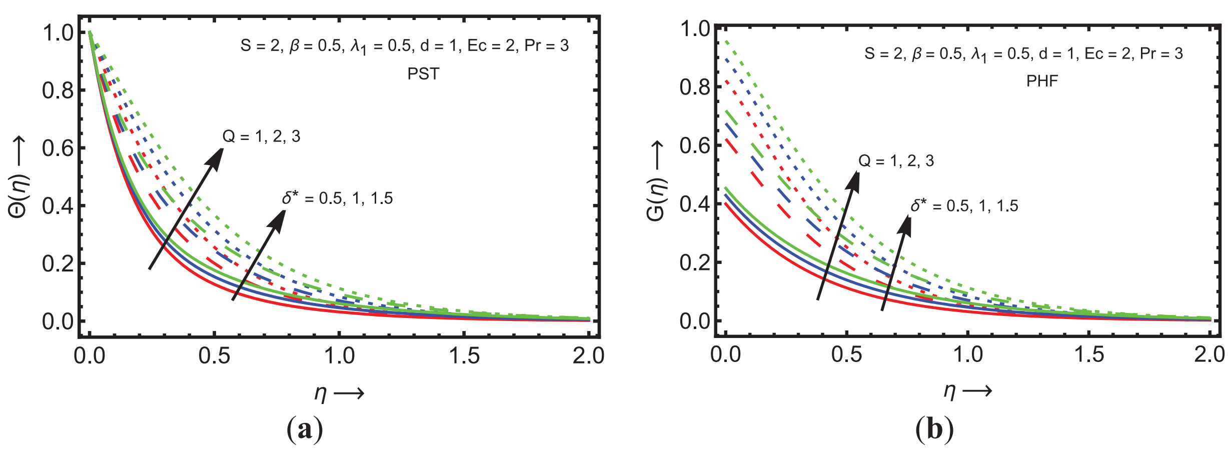

Figure 7: (**a**) Impact of δ^* and Q on $\Theta(\eta)$. Where colours show δ^* variation and different types of lines show Q variation; (**b**) Impact of δ^* and Q on $G(\eta)$. Where colours show δ^* variation and different types of lines show Q variation

Fig. 8a,b presents the temperature distribution for the PST and PHF cases, respectively, along with the effects of the Eckert number and δ^*. A higher Eckert number results in an expanded thermal boundary layer, increasing the significance of dissipative energy and broadening the temperature profile. Additionally, energy dissipation causes a sharper temperature gradient in the PST case and a rise in wall temperature in the PHF case. Energy dissipation from electrical resistance generates a larger temperature field and an increase in the Eckert number. Notably, there is a considerable temperature overshoot as the Eckert number increases, reflecting the relationship between the flow's kinetic energy and the enthalpy difference in the boundary layer. Internal friction heating between fluid molecules, combined with ohmic heating, which converts mechanical and electrical energy into thermal energy, heats the fluid in the stretching sheet flow. A higher δ^* and Eckert number produces more thermal energy, resulting in a higher temperature of the stretched sheet and a thicker thermal boundary layer.

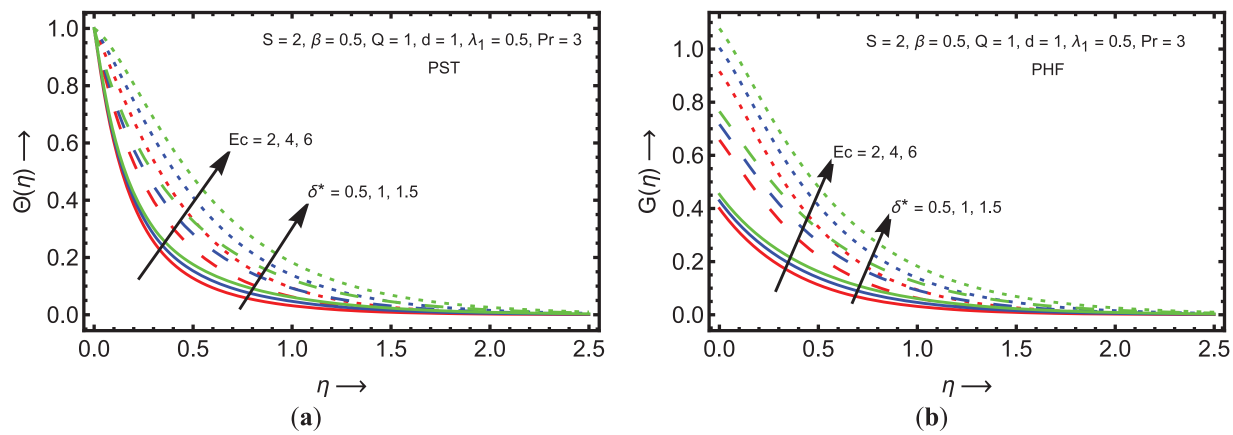

Figure 8: (**a**) Impact of δ^* and Ec on $\Theta(\eta)$. Where colours show δ^* variation and different types of lines show Ec variation; (**b**) Impact of δ^* and Ec on $G(\eta)$. Where colours show δ^* variation and different types of lines show Ec variation

5.5 Local Nusselt Number and Dimensionless Temperature Results

Fig. 9 shows the variation of the local Nusselt number for different parameters, including λ_1, β, and δ^*. Fig. 9a shows that as the λ_1 grows, so does the local Nusselt number. As retardation time grows, the fluid has more time to absorb heat, resulting in a larger temperature differential at the surface and consequently a higher local Nusselt number, which decreases with Q.

Fig. 9b demonstrates the behavior of the local Nusselt number in relation to the Q for different values of the β. It has been noted that an increase in the β results in a decrease in the local Nusselt number. Fig. 9c illustrates that as δ^* increases, the local Nusselt number decreases, thereby enhancing heat transfer within the boundary layer. Fig. 10 depicts the relationship between $\frac{1}{G(0)}$ which is a local Nusselt number for the PHF case and the Q. Fig. 10a demonstrates that when λ_1 increases, the $\frac{1}{G(0)}$ value rises significantly since it is the reciprocal of the temperature profile in the PHF case $(\eta = 0)$. Fig. 10b,c shows the $\frac{1}{G(0)}$ values drop when the β and δ^* rise, respectively. This small drop is caused by the magnetic field. An increase in the Q increases the Lorentz force, which opposes fluid motion and reduces the temperature gradient, hence decreasing the $\frac{1}{G(0)}$ value due to the Lorents force. Table 3 shows the non-dimensional temperature profiles for the PST and PHF cases, along with the local Nusselt numbers for both cases, under different parameters such as λ_1, β, δ^*, Q, Eckert number, and Pr.

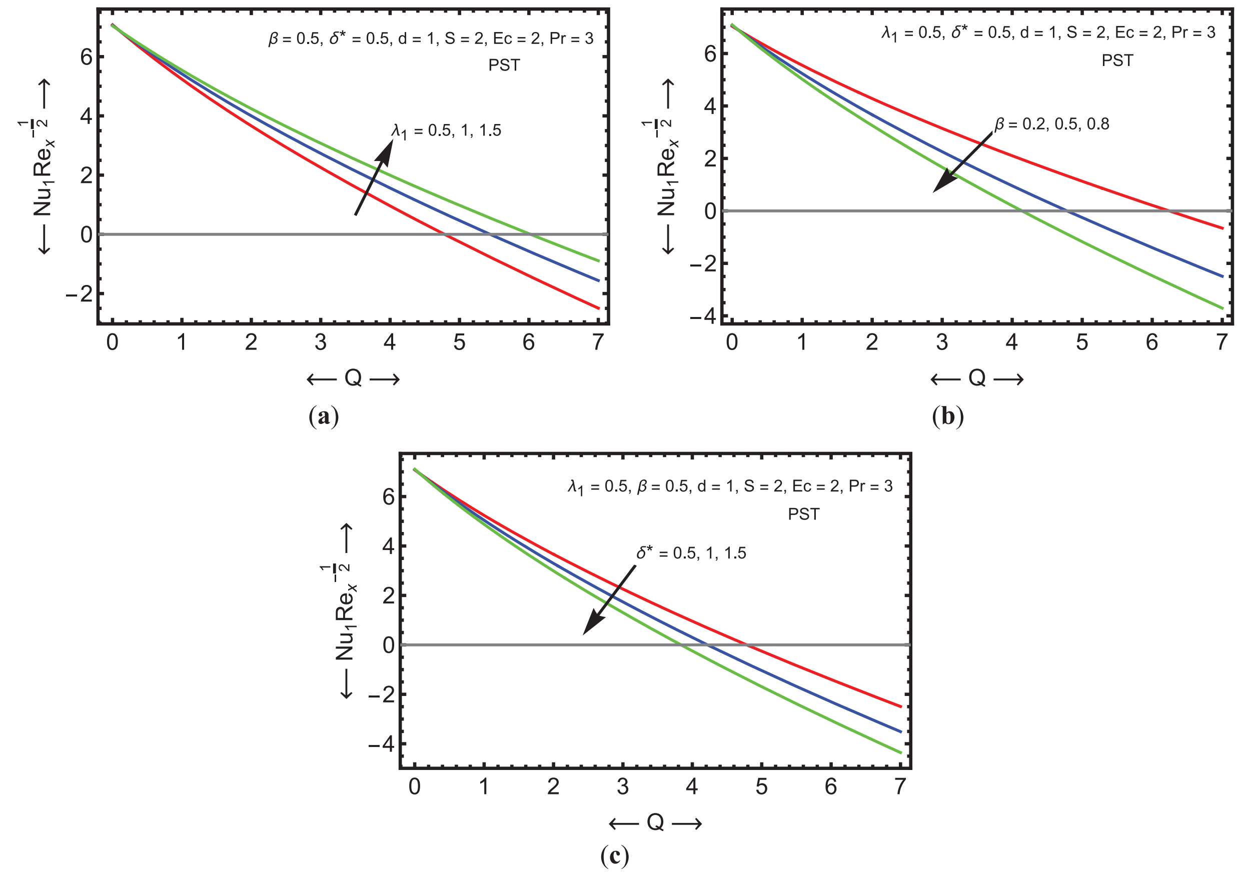

Figure 9: (**a**) Impact of λ_1 on domain local Nusselt number $Nu_1\,\mathrm{Re}_x^{-(1/2)}$ as a function of Q; (**b**) Impact of β on domain local Nusselt number $Nu_1\,\mathrm{Re}_x^{-(1/2)}$ as a function of Q; (**c**) Impact of δ^* on domain local Nusselt number $Nu_1\,\mathrm{Re}_x^{-(1/2)}$ as a function of Q

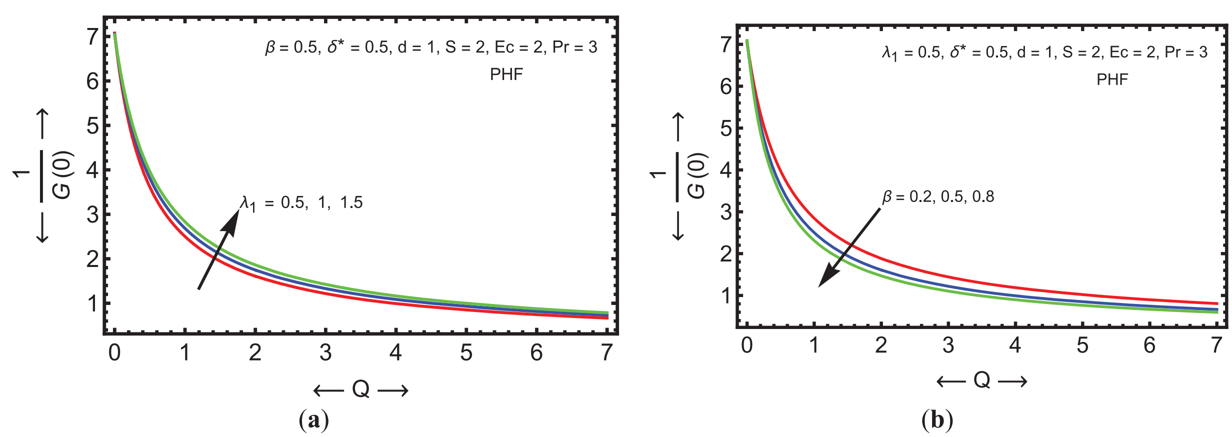

Figure 10: (Continued)

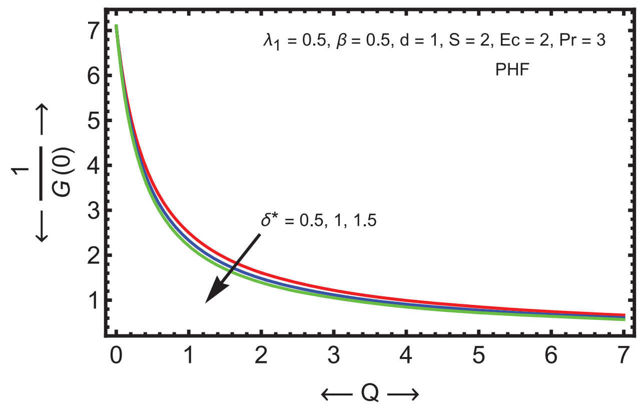

(**c**)

Figure 10: (**a**) Impact of λ_1 and Q on $\frac{1}{G(0)}$; (**b**) Impact of β and Q on $\frac{1}{G(0)}$; (**c**) Impact of δ^* and Q on $\frac{1}{G(0)}$

Table 3: Numerical values of $\Theta_\eta(0)$, $G(0)$, $Nu_1 \mathrm{Re}_x^{-(1/2)}$ and $Nu_2 \mathrm{Re}_x^{-(1/2)}$ for various values of λ_1, β, δ^*, Q, Ec and Pr

Parameters	Values	$\Theta_\eta(0)$	$G(0)$	$Nu_1 \mathrm{Re}_x^{-(1/2)}$	$Nu_2 \mathrm{Re}_x^{-(1/2)}$
λ_1	0.5	−5.2370225	0.3998210	5.2370225	2.5011191
	1.0	−5.4156244	0.3727043	5.4156244	2.6830921
	1.5	−5.5413498	0.3532163	5.5413498	2.8311264
β	0.2	−5.5523059	0.3514982	5.5523059	2.8449645
	0.5	−5.2370225	0.3998210	5.2370225	2.5011191
	0.8	−5.0221945	0.4318190	5.0221945	2.3157850
δ^*	0.5	−5.2370225	0.3998210	5.2370225	2.5011191
	1.0	−5.0405438	0.4291067	5.0405438	2.3304227
	1.5	−4.8766114	0.4532263	4.8766114	2.2064031
Q	1.0	−5.2370225	0.3998210	5.2370225	2.5011191
	2.0	−3.6654081	0.6217406	3.6654081	1.6083878
	3.0	−2.2557324	0.8215185	2.2557324	1.2172580
Ec	2.0	−5.2370225	0.3998210	5.2370225	2.5011191
	4.0	−3.4144466	0.6579909	3.4144466	1.5197778
	6.0	−1.5918708	0.9161608	1.5918708	1.0915114
Pr	3.0	−5.2370225	0.3998210	5.2370225	2.5011191
	5.0	−8.2148024	0.3547709	8.2148024	2.8187205
	8.0	−12.6049861	0.3281504	12.6049861	3.0473835

6 Conclusion

The present analytical investigation studied the impact of MFD viscosity on the Jeffrey fluid flow with ohmic dissipation over a stretching surface, using defined boundary conditions. The velocity and temperature profiles for the PST and PHF cases were examined, and the non-dimensional differential equations were solved through the use of a confluent hypergeometric function. The study examined various physical parameters, including the δ^*, Q, λ_1, β, Eckert number, and Pr, with detailed graphical discussions of their impact on thermal behavior. The main conclusions are as follows:

- The study employs similarity transformations to convert nonlinear partial differential equations into ordinary differential equations, and obtained the unique solution to momentum equations, which are solved analytically using a confluent hypergeometric function.
- The velocity of the Jeffrey fluid decreases with increasing retardation time and magnetic interaction parameter, as a thinner velocity boundary layer develops. Conversely, higher magnetic viscosity and Deborah number enhances fluid velocity due to reduced resistance.
- The local skin friction coefficient rises with retardation time, but decreases with Deborah number, magnetic interaction parameter, and magnetic viscosity, suggesting complex interactions between fluid movement and these parameters.
- The increased retardation time lowers the temperature distribution due to the thinning of the thermal boundary region, whereas higher magnetic interaction, magnetic viscosity, and Deborah number elevate the temperature in both PST and PHF cases.
- An increase in retardation time increases the local Nusselt number, indicating improved heat transfer, while increases in magnetic viscosity and Deborah number generally decrease the Nusselt number.
- This work not only enhances the understanding of Jeffrey fluid behavior in MFD environments but also provides analytical solutions for comparing future numerical and analytical works on the impacts of MFD on Jeffrey fluid boundary layer flow.

Acknowledgement: The authors sincerely thank the honorable referees and the editor for their valuable comments and suggestions, which have significantly improved the quality of this paper.

Funding Statement: This research was financially supported by the United Arab Emirates University, Al Ain, United Arab Emirates, under Grant No. 12R283.

Author Contributions: K. Sinivasan: Writing—original draft, Visualization, Validation, Methodology, Formal analysis, Conceptualization. N. Vishnu Ganesh: Writing—review & editing, Writing—original draft, Validation, Methodology, Investigation, Formal analysis, Conceptualization. G. Hirankumar: Writing—review & editing, Supervision, Methodology, Formal analysis, Conceptualization. M. Al-Mdallal Qasem: Writing—review & editing, Software, Methodology, Funding acquisition, Conceptualization. All authors reviewed the results and approved the final version of the manuscript.

Availability of Data and Materials: The data that support the findings of this study are available upon reasonable request from the authors.

Ethics Approval: Not applicable.

Conflicts of Interest: The authors declare no conflicts of interest to report regarding the present study.

Nomenclature

A	Extra stress tensor
A_0 and E_0	Constants whose value depend on the properties of the fluid
B_0	Strength of magnetic field
b	Linear stretching rate constant
C_f	Skin friction coefficient
c_p	Specific heat capacity at constant pressure $\left(\mathrm{Jkg^{-1}K^{-1}}\right)$
d	Constant

Ec_1 and Ec_2	$\left(Ec_1 = \frac{b^2 l^2}{A_0 c_p}\right.$ and $\left.Ec_2 = \frac{\kappa b^2 l^2}{E_0 c_p}\sqrt{\frac{b}{\nu}}\right)$ Eckert number
κ	Thermal conductivity of the fluid $\left(\mathrm{Wm^{-1}K^{-1}}\right)$
l	Characteristic length
M	Kummer's function (or) Confluent hypergeometric function
p	Pressure
Pr	$\left(= \frac{\mu c_p}{\kappa}\right)$ Prandtl number
Q	$\left(= \frac{\sigma B_0^2}{b\rho}\right)$ Magnetic interaction parameter
q_w	Heat transfer rate at the surface flux $\left(\mathrm{Wm^{-2}}\right)$
R_1	Rivlin-Ericksen tensor
$\mathrm{Re}_x^{1/2}$	$\left(= \frac{b^{1/2} x}{\nu^{1/2}}\right)$ local Reynolds number
S	Suction and blowing parameter as $S > 0$ and $S < 0$, respectively
$\tilde{T}$	Temperature (K)
$\tilde{T}_\infty$	Temperature away from the sheet (K)
$\tilde{T}_w$	Wall temperature of the sheet (K)
u^* and v^*	velocity components in the x and y directions $\left(\mathrm{ms^{-1}}\right)$
u_w	Stretching velocity $\left(\mathrm{ms^{-1}}\right)$
v_w	Permeability of the stretching sheet
x and y	System of coordinates (m)

Greek Symbols

α	Solution domain
β	$(= \lambda_2 b)$ is the Deborah number
δ^*	$(= \delta B_0)$ Magnetic viscosity parameter
η	Similarity variable
λ_1	Ratio of relaxation to retardation times
λ_2	Relaxation time
μ	Viscosity of the fluid $\left(\mathrm{kgm^{-1}s^{-1}}\right)$
ν	Kinematic viscosity $\left(\mathrm{m^2s^{-1}}\right)$
ρ	Density of the fluid $\left(\mathrm{kgm^{-3}}\right)$
σ	Electrical conductivity $\left(\mathrm{Sm^{-1}}\right)$
τ^*	Cauchy stress tensor
Θ	Non-dimensional temperature

Superscript

t^*	Transpose

Subscripts

w	Quantities at wall
x	Differentiation with respect to x
y	Differentiation with respect to y
∞	Quantities at free stream
η	Differentiation with respect to η

Abbreviations

MFD	Magnetic field dependent
MHD	Magnetohydrodynamics
PST	Prescribed surface temperature
PHF	Prescribed heat flux

References

1. Jeffery GBL. The two-dimensional steady motion of a viscous fluid. Lond Edinb Dublin Philos Mag J Sci. 1915;29(172):455–65. doi:10.1080/14786440408635327.
2. Vajravelu K, Rollins D. Heat transfer in a viscoelastic fluid over a stretching sheet. J Math Anal Appl. 1991;158(1):241–55. doi:10.1016/0022-247X(91)90280-D.
3. Hayat T, Asad S, Qasim M, Hendi AA. Boundary layer flow of a Jeffrey fluid with convective boundary conditions. Int J Numer Methods Fluids. 2012;69(8):1350–62. doi:10.1002/fld.2642.
4. Qasim M. Heat and mass transfer in a Jeffrey fluid over a stretching sheet with heat source/sink. Alex Eng J. 2013;52(4):571–5. doi:10.1016/j.aej.2013.08.004.
5. Turkyilmazoglu M, Pop I. Exact analytical solutions for the flow and heat transfer near the stagnation point on a stretching/shrinking sheet in a Jeffrey fluid. Int J Heat Mass Transf. 2013;57(1):82–8. doi:10.1016/j.ijheatmasstransfer.2012.10.006.
6. Nadeem S, Haq RU, Khan ZH. Numerical study of MHD boundary layer flow of a Maxwell fluid past a stretching sheet in the presence of nanoparticles. J Taiwan Inst Chem Eng. 2014;45(1):121–6. doi:10.1016/j.jtice.2013.04.006.
7. Pramanik S. Casson fluid flow and heat transfer past an exponentially porous stretching surface in presence of thermal radiation. Ain Shams Eng J. 2014;5(1):205–12. doi:10.1016/j.asej.2013.05.003.
8. Dalir N. Numerical study of entropy generation for forced convection flow and heat transfer of a Jeffrey fluid over a stretching sheet. Alex Eng J. 2014;53(4):769–78. doi:10.1016/j.aej.2014.08.005.
9. Kumar M. Study of differential transform technique for transient hydromagnetic Jeffrey fluid flow from a stretching sheet. Nonlinear Eng. 2020;9(1):145–55. doi:10.1515/nleng-2020-0004.
10. Ahmad K, Ishak A. MHD flow and heat transfer of a Jeffrey fluid over a stretching sheet with viscous dissipation. Malays J Math Sci. 2016;10:311–23.
11. Ahmed J, Bourazza S, Sarfraz M, Orsud MA, Eldin SM, Askar NA, et al. Heat transfer in Jeffrey fluid flow over a power law lubricated surface inspired by solar radiations and magnetic flux. Case Stud Therm Eng. 2023;49(10):103220. doi:10.1016/j.csite.2023.103220.
12. Dharmaiah G, Mebarek-Oudina F, Prasad JR, Rani CB. Exploration of bio-convection for slippery two-phase Maxwell nanofluid past a vertical induced magnetic stretching regime associated for biotechnology and engineering. J Mol Liq. 2023;391(1):123408. doi:10.1016/j.molliq.2023.123408.
13. Ajithkumar M, Kuharat S, Bég OA, Sucharitha G, Lakshminarayana P. Catalytic effects on peristaltic flow of Jeffrey fluid through a flexible porous duct under oblique magnetic field: application in biomimetic pumps for hazardous materials. Therm Sci Eng Prog. 2024;49(4):102476. doi:10.1016/j.tsep.2024.102476.
14. Ramesh K, Vemulawada S, Khan SU, Saleem S, Sharma A, Lodhi RK, et al. Peristaltic propulsion of Jeffrey nanofluid with heat and electromagnetic effects: application to biomedicine. Multiscale Multidiscip Model Exp Des. 2024;7(6):6151–70. doi:10.1007/s41939-024-00572-7.
15. Chillingo KJ, Onyango ER, Matao PM. Influence of induced magnetic field and chemically reacting on hydromagnetic Couette flow of Jeffrey fluid in an inclined channel with variable viscosity and convective cooling: a Caputo derivative approach. Int J Thermofluids. 2024;22(3):100627. doi:10.1016/j.ijft.2024.100627.
16. Babu DH, Narayana PS. Joule heating effects on MHD mixed convection of a Jeffrey fluid over a stretching sheet with power law heat flux: a numerical study. J Magn Magn Mater. 2016;412(1):185–93. doi:10.1016/j.jmmm.2016.04.011.
17. Thumma T, Mishra SR. Effect of viscous dissipation and Joule heating on magnetohydrodynamic Jeffery nanofluid flow with and without multi slip boundary conditions. J Nanofluids. 2018;7(3):516–26. doi:10.1166/jon.2018.1469.
18. Muzara H, Shateyi S. MHD laminar boundary layer flow of a Jeffrey fluid past a vertical plate influenced by viscous dissipation and a heat source/sink. Mathematics. 2021;9(16):1896. doi:10.3390/math9161896.
19. Pal D, Mondal S, Mondal H. Entropy generation on MHD Jeffrey nanofluid over a stretching sheet with nonlinear thermal radiation using spectral quasilinearization method. Int J Ambient Energy. 2021;42(15):1712–26. doi:10.1080/01430750.2019.1614984.

20. Kausar MS, Al-Sharifi HAM, Hussanan A, Mamat M. The effects of thermal radiation and viscous dissipation on the stagnation point flow of a micropolar fluid over a permeable stretching sheet in the presence of porous dissipation. J Fluid Dyn Mater Process. 2022;19(1):61–81. doi:10.32604/fdmp.2023.021590.
21. Pal D, Mondal S. Analysis of entropy generation on mhd radiative viscous-ohmic dissipative heat transfer over a stretching sheet in a chemically reactive Jeffrey nanofluid with non-uniform heat source/sink based on SQLM. J Nanofluids. 2023;12(7):1903–20. doi:10.1166/jon.2023.2096.
22. Abuiyada A, Eldabe N, Abouzeid M, Elshaboury S. Influence of both Ohmic dissipation and activation energy on peristaltic transport of Jeffery nanofluid through a porous media. CFD Lett. 2023;15(6):65–85. doi:10.37934/cfdl.15.6.6585.
23. Raje A, Bhise AA, Kulkarni A. Entropy analysis of the MHD Jeffrey fluid flow in an inclined porous pipe with convective boundaries. Int J Thermofluids. 2023;17(03):100275. doi:10.1016/j.ijft.2022.100275.
24. Trivedi M, Otegbeye O, Ansari MS, Fayaz T. Flow of Jeffrey fluid near impulsively moving plate with nanoparticle and activation energy. Int J Thermofluids. 2023;18(2):100354. doi:10.1016/j.ijft.2023.100354.
25. Elboughdiri N, Javid K, Lakshminarayana P, Abbasi A, Benguerba Y. Effects of Joule heating and viscous dissipation on EMHD boundary layer rheology of viscoelastic fluid over an inclined plate. Case Stud Therm Eng. 2024;60:104602. doi:10.1016/j.csite.2024.104602.
26. Riaz MB, Rehman AU, Chan CK, Zafar AA, Tunç O. Thermal and flow properties of Jeffrey fluid through prabhakar fractional approach: investigating heat and mass transfer with emphasis on special functions. Int J Appl Comput Math. 2024;10(3):111. doi:10.1007/s40819-024-01747-z.
27. Afifi MD, Jahangiri A, Ameri M. Numerical and analytical investigation of Jeffrey nanofluid convective flow in magnetic field by FEM and AGM. Int J Thermofluids. 2024;25(11):100999. doi:10.1016/j.ijft.2024.100999.
28. Dharmaiah G, Mebarek-Oudina F, Balamurugan KS, Vedavathi N. Numerical analysis of the magnetic dipole effect on a radiative ferromagnetic liquid flowing over a porous stretched sheet. Fluid Dyn Mater Process. 2024;20(2):293–310. doi:10.32604/fdmp.2023.030325.
29. Kumar MA, Mebarek-Oudina F, Mangathai P, Shah NA, Vijayabhaskar C, Venkatesh N, et al. The impact of Soret Dufour and radiation on the laminar flow of a rotating liquid past a porous plate via chemical reaction. Mod Phys Lett B. 2025;39(10):2450458. doi:10.1142/S021798492450458X.
30. Alsaedi A, Iqbal Z, Mustafa M, Hayat T. Exact solutions for the magnetohydrodynamic flow of a Jeffrey fluid with convective boundary conditions and chemical reaction. Z Für Naturforschung A. 2012;67(8–9):517–24. doi:10.5560/zna.2012-0054.
31. Ahmed J, Shahzad A, Khan M, Ali R. A note on convective heat transfer of an MHD Jeffrey fluid over a stretching sheet. AIP Adv. 2015;5(11):117117. doi:10.1063/1.4935571.
32. Hayat T, Asad S, Mustafa M, Alsaedi A. MHD stagnation-point flow of Jeffrey fluid over a convectively heated stretching sheet. Comput Fluids. 2015;108:179–85. doi:10.1016/j.compfluid.2014.11.016.
33. Turkyilmazoglu M. Magnetic field and slip effects on the flow and heat transfer of stagnation point Jeffrey fluid over deformable surfaces. Z Für Naturforschung A. 2016;71(6):549–56. doi:10.1515/zna-2016-0047.
34. Kumar PV, Ibrahim SM, Lorenzini G. Impact of thermal radiation and Joule heating on MHD mixed convection flow of a Jeffrey fluid over a stretching sheet using homotopy analysis method. Int J Heat Technol. 2017;35(4):978–86. doi:10.18280/ijht.350434.
35. Nisar KS, Mohapatra R, Mishra SR, Reddy MG. Semi-analytical solution of MHD free convective Jeffrey fluid flow in the presence of heat source and chemical reaction. Ain Shams Eng J. 2021;12(1):837–45. doi:10.1016/j.asej.2020.08.015.
36. Sheikholeslami M, Rashidi MM, Hayat T, Ganji DD. Free convection of magnetic nanofluid considering MFD viscosity effect. J Mol Liq. 2016;218(8):393–9. doi:10.1016/j.molliq.2016.02.093.
37. Sheikholeslami M, Sadoughi MK. Numerical modeling for Fe_3O_4-water nanofluid flow in porous medium considering MFD viscosity. J Mol Liq. 2017;242(9):255–64. doi:10.1016/j.molliq.2017.07.004.
38. Molana M, Dogonchi AS, Armaghani T, Chamkha AJ, Ganji DD, Tlili I. Investigation of hydrothermal behavior of Fe_3O_4-H_2O nanofluid natural convection in a novel shape of porous cavity subjected to magnetic field dependent (MFD) viscosity. J Energy Storage. 2020;30(3):101395. doi:10.1016/j.est.2020.101395.

39. Ganesh NV, Rajesh B, Al-Mdallal QM, Muzara H. Influence of magnetic field-dependent viscosity on Casson-based nanofluid boundary layers: a comprehensive analysis using Lie group and spectral quasilinearization method. Heliyon. 2024;10(7):28994. doi:10.1016/j.heliyon.2024.e28994.
40. Ganesh NV, Sinivasan K, Al-Mdallal QM, Hirankumar G. An analytical study on the influence of magnetic field-dependent viscosity on viscous and ohmic dissipative second-grade fluid boundary layers. Phys Scr. 2024;99(7):075219. doi:10.1088/1402-4896/ad4f75.